Letter

Anna Labno, Christopher Gladden, Jeongmin Kim, Dylan Lu, Xiaobo Yin, Yuan Wang, Zhaowei Liu* and Xiang Zhang*

Three-dimensional nanoscale imaging by plasmonic Brownian microscopy

https://doi.org/10.1515/nanoph-2017-0075
Received July 21, 2017; revised October 1, 2017; accepted October 31, 2017

Abstract: Three-dimensional (3D) imaging at the nanoscale is a key to understanding of nanomaterials and complex systems. While scanning probe microscopy (SPM) has been the workhorse of nanoscale metrology, its slow scanning speed by a single probe tip can limit the application of SPM to wide-field imaging of 3D complex nanostructures. Both electron microscopy and optical tomography allow 3D imaging, but are limited to the use in vacuum environment due to electron scattering and to optical resolution in micron scales, respectively. Here we demonstrate plasmonic Brownian microscopy (PBM) as a way to improve the imaging speed of SPM. Unlike photonic force microscopy where a single trapped particle is used for a serial scanning, PBM utilizes a massive number of plasmonic nanoparticles (NPs) under Brownian diffusion in solution to scan in parallel around the unlabeled sample object. The motion of NPs under an evanescent field is three-dimensionally localized to reconstruct the super-resolution topology of 3D dielectric objects. Our method allows high throughput imaging of complex 3D structures over a large field of view, even with internal structures such as cavities that cannot be accessed by conventional mechanical tips in SPM.

Keywords: 3D nano-imaging; Brownian motion; microscopy; parallel scanning; evanescent field.

1 Introduction

Three-dimensional (3D) imaging at the nanoscale is critical to study nanomaterials and complex systems. Scanning probe microscopy (SPM) such as atomic force microscopy (AFM) and near-field scanning optical microscopy (NSOM) is a commonly used and powerful imaging technique that offers nanometer resolution, but is limited to imaging the surface topology of a small area due to the serial scanning nature of a single tip [1, 2]. Tip arrays have been pursued to increase the SPM throughput [3, 4], but laborious engineering and control of individual tips are required to maintain the nanometer distance between each tip and surface. Also, precise shaping of the tip geometry by etching [5, 6] or functionalization with carbon nanotubes [7] enables SPM to image nanostructures with a higher aspect ratio, but the technique still cannot image 3D overhanging structures and cavities, as well as soft samples like biological materials. This limited imaging capability was well addressed by photonic force microscopy (PFM) [8, 9] that replaces the conventional stiff probe with an optically trapped, sub-micron-sized particle as a soft probe. While PFM demonstrated truly 3D imaging of transparent (biological) objects, its imaging speed dependent on a single probe is still inherently slow. On the other hand, electron microscopy allows wide-field 3D imaging of nanoscale structures at higher speed but often requires vacuum environment with limited imaging penetration due to electron scattering. Optical tomography and time reversal technique may be an alternative wide-field 3D imaging method, yet exhibit lower spatial resolution in microns due to the diffraction limit [10–12]. Plasmonic superlens [13–16] enables super-resolution optical

***Corresponding authors: Zhaowei Liu,** Department of Electrical and Computer Engineering, University of California, 9500 Gilman Drive, La Jolla, San Diego, CA 92093, USA, e-mail: zhaowei@ucsd.edu; and **Xiang Zhang,** NSF Nanoscale Science and Engineering Center (NSEC), University of California, 3112 Etcheverry Hall, Berkeley, CA 94720, USA; and Materials Sciences Division, Lawrence Berkeley National Laboratory, 1 Cyclotron Road, Berkeley, CA 94720, USA, e-mail: xiang@berkeley.edu.
Anna Labno, Christopher Gladden, Jeongmin Kim and Xiaobo Yin: NSF Nanoscale Science and Engineering Center (NSEC), University of California, Berkeley, CA 94720, USA
Dylan Lu: Department of Electrical and Computer Engineering, University of California, San Diego, CA 92093, USA
Yuan Wang: NSF Nanoscale Science and Engineering Center (NSEC), University of California, Berkeley, CA 94720, USA; and Materials Sciences Division, Lawrence Berkeley National Laboratory, Berkeley, CA 94720, USA

imaging beyond the diffraction limit but only provides two-dimensional imaging at a smaller area [17]. Single molecule localization microscopy (SMLM) allows 3D imaging of complex objects with nanometer accuracy, but requires the samples labeled with emitter molecules such as fluorophores and quantum dots [18–21]. The staining requirement makes SMLM primarily applicable to biological objects with known molecular identities.

Here, we demonstrate a new imaging technique, plasmonic Brownian microscopy (PBM), based on fast, massively parallel stochastic scanning of 3D nano-objects with plasmonic nanoparticles (NPs). Our method is somewhat similar to PFM, but relies on a number of NPs as multiple scanning probes free from optical tweezers as a way to enhance the imaging speed in SPM. An object surrounded by these freely diffusing NPs is placed in an evanescent field, supported by total-internal-reflection (TIR) illumination, where the scattering intensity of resonant NPs determines their vertical location. The positions of the NPs can therefore be localized in all three dimensions and the voxels unoccupied by these NPs form the 3D shape of the object. We show that our approach has a resolving power of laterally 30 nm for an isolated line object and axially 30 nm for a staircase object. This wide-field, super-resolution imaging technique is also capable of imaging unlabeled, low contrast objects such as complex nanostructures with overhangs and internal structures in a liquid environment. Realizing a massive number of SPM tips in parallel, PBM holds great potential for large-scale imaging of unlabeled 3D nanostructures over a large field of view.

In PBM, an object of arbitrary shape is placed in solution of randomly diffusing NPs, and a series of images are acquired. These freely diffusing particles have to be captured rapidly in a camera before they diffuse a significant distance. To allow a shorter exposure time of image acquisition, we use the 50 nm gold NPs excited near their plasmon resonance at 532 nm where strong scattering signals are produced without bleaching or saturation. The resonant scattering enables us to collect a sufficient number of photons per particle to accurately localize its position. The whole NPs are individually localized in three dimensions as they probe the volume around the object by Brownian diffusion (Figure 1A). The scattering intensity depends sensitively on the exponentially decaying electromagnetic field and can be used to precisely determine the vertical position. The lateral position of the particle is found by fitting the particle's image with a two-dimensional Gaussian function. An accumulation of these high-precision localization data maps out the space excluded by the object, and thus enables us to reconstruct a three-dimensional object with resolution down to nanometers (Figure 1B). In comparison with conventional SPM, PBM that uses massively parallel NP probes is not only high throughput and wide field, but also can access underneath nanoscale objects with overhangs and cavities.

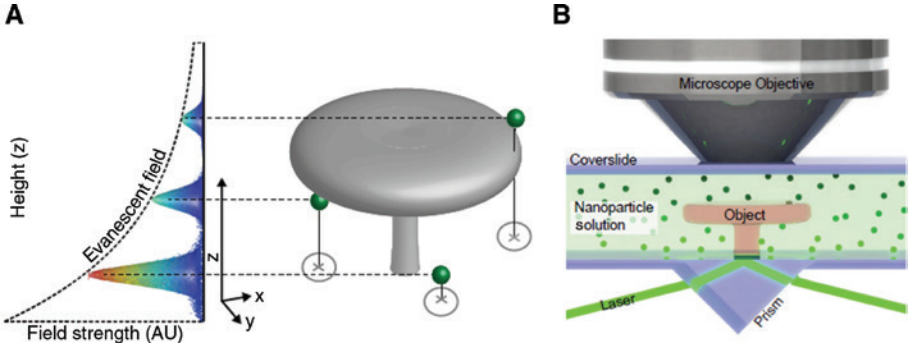

Figure 1: Principle of the PBM technique.
(A) PBM relies on three-dimensional localization of freely diffusing NPs based on the correlation between evanescent field intensity and height. An object of arbitrary shape (gray) is placed in a solution of randomly diffusing nanoparticles (green spheres), which are illuminated by an evanescent field established by total internal reflection (TIR) at the interface between the substrate and the object. A series of raw images of the particle's scattering are acquired and the NPs are individually localized in three dimensions as they probe the volume around the object by Brownian diffusion. Images taken at different times record different NPs randomly distributed around the object. The lateral localization is obtained by 2D Gaussian fitting, while the height of particle is estimated by measuring the intensity of the scattering signal. Since the evanescent field decays exponentially with the distance from the interface, the NPs close to the interface will interact with a stronger field and appear brighter than ones further away. Space occupied by the object is inaccessible to the NPs, and the excluded volume corresponds to the object. (B) Experimental setup. The sample, composed of sapphire cover slip with a PMMA structure, is enclosed in a chamber filled with a low-density solution of 50 nm gold NPs whose index is matched to the sample. The chamber is illuminated with a laser and the NP scattering signal is detected using a 100× oil immersion objective.

2 Results and discussion

We fabricated 3D staircase structures consisting of three steps with a height of 30 nm, 35 nm and 40 nm, respectively (Figure 2A and B). The structure is made of poly(methyl methacrylate) (PMMA) and was imaged using PBM in a flow chamber filled with freely diffusing 50 nm gold NPs with topside TIR illumination (200 mW, 532 nm laser) on an inverted microscope (Figure 2C). The entire structure, including height at each point, was imaged by the massively parallel scanning of NPs. The smallest height separation between two steps is 30 nm and can be accurately imaged in agreement with AFM measurements (Figure 2D). Figure 2E shows a reconstructed image of a 100-nm-height PMMA square pad object under a refractive index mismatch of 0.058 between PMMA and NP solution, whose mismatch is larger than an index variation within typical biological structures in a cellular level. While such an index mismatch may cause an additional axial error due to the altered penetration depth of the evanescent field formed on the sample, our experimental result still showed a quality image. In fact, our full wave simulation (see Supplementary Figure S2) estimated less than 10 nm axial error for $\Delta n = 0.06$. The index mismatch could also affect lateral localization precision for those NPs at nearby side walls of or underneath the object, due to optical aberrations that can induce lateral shifts of point spread functions (PSFs) or rotationally asymmetric PSFs. These aberrations are expected to be much smaller than the wavelength for our demonstrated objects (<100 nm in height) with $\Delta n = 0.058$ and thus neglected here. However, one needs to be aware of a potentially undesirable influence of optical aberrations on localization precision.

In addition, we imaged a "Cal Nano" nanostructure made by e-beam lithography (Figure 3A and B), which contains diverse feature sizes. We use Figure 3 to demonstrate the capability of our technique to image complex structures with a smallest gap width around 100 nm. PBM not only captures the full three-dimensional nature of the structure (Figure 3C) but also features as small as 100 nm over an entire $30 \times 30\ \mu m^2$ field of view (Figure 3D). Figure 3E/F shows a number of lines of progressively decreasing width ranging from 120 nm down to 20 nm separated by 100 nm gaps (corresponding to a

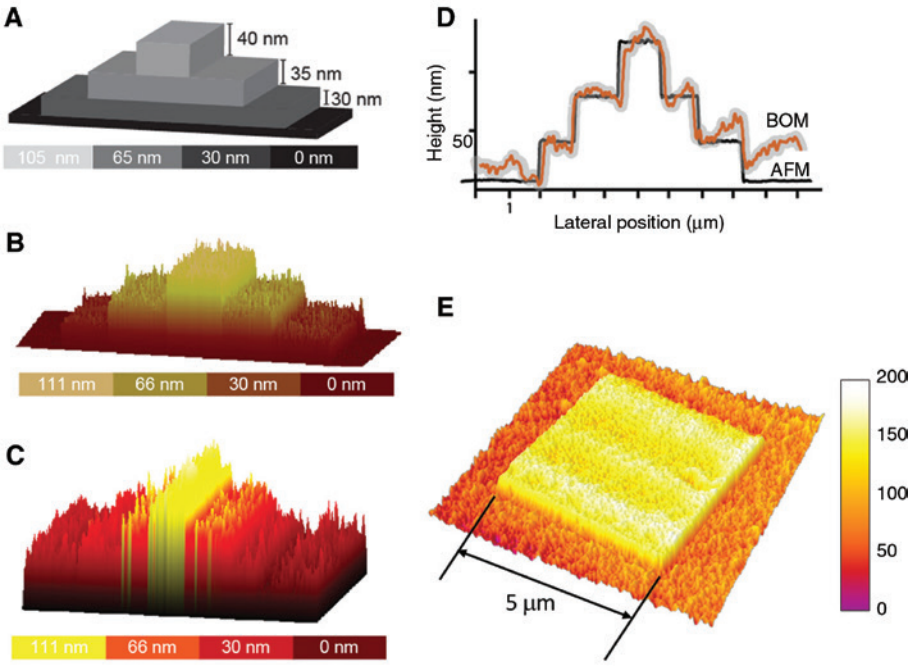

Figure 2: PBM can achieve 30 nm vertical resolution.
(A) Schematic of a staircase PMMA object on a sapphire substrate. The sample consists of three steps with 30 nm, 35 nm and 40 nm height, respectively. (B) AFM image of the sample clearly shows three different levels. (C) PBM image of the same sample showing three distinct steps. This PBM image was reconstructed from 100,000 frames collected. (D) Averaged cross section of the AFM (black) and PBM images (orange) showing that PBM accurately detected the heights of the steps with under 30 nm sensitivity. The gray overlay around the orange line indicates the standard deviation of the heights along the cross section. On the right-hand side of the staircase, the PBM reconstruction indicates higher step height than AFM does due to uneven illumination; the rest however matches very well with the AFM result. (E) PBM image of a $5\ \mu m \times 5\ \mu m$ PMMA square pad with 100 nm height when the solution index is not matched with the sample ($\Delta n = 0.058$).

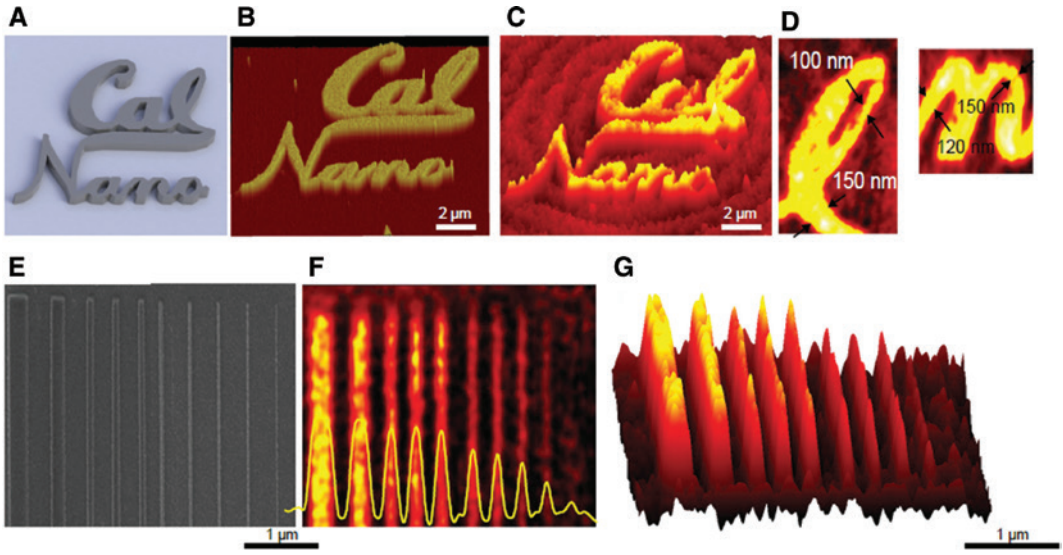

Figure 3: PBM can image three-dimensional topology of complex shapes with 30 nm feature size.
(A) Schematics of an extruded "CalNano" shape fabricated out of PMMA by e-beam lithography. The surface of the PMMA is 120 nm above the sapphire surface. (B) AFM image shows also a few NPs stuck to the sample after an experiment. (C) Three-dimensional PBM image in which the CalNano pattern's geometry is clearly resolved. The whole 10 µm × 10 µm image was acquired by collecting 200,000 frames, each with an acquisition time of 3 ms. (D) Zoom-in highlighting the ability of PBM to resolve 100–150 nm features in the letters "l" and "n". (E) SEM of fabricated lines with progressively decreasing width and height. The width of the lines, each separated by 100 nm, ranges from 120 nm on left-hand side to 20 nm on the right-hand side. (F) PBM image of the lines including the averaged cross section (yellow) showing that the smallest 30 nm line is clearly visible, while the 20 nm line is only barely visible. (G) Three-dimensional reconstruction of the line sample showing both the varying thickness of the lines, all the way down to the 30 nm line, and the decreasing height of the lines.

grating constant of 200 nm). As shown in Figure 3F/G, PBM shows a lateral sensitivity down to 30 nm for an isolated line object. Each dip between the isolated lines can be clearly resolved as long as the dip is wider than the diameter of NPs.

Finally, we demonstrate that PBM can image the topology of a three-dimensional object with internal geometry, such as overhung structures or cavities. A structure consisting of a silicon dioxide layer on a sapphire substrate was patterned into a smiley face that is roofed by an overhanging structure made of PMMA (Figure 4A). This structure is difficult to image with SEM due to the fact that the top thick PMMA layer shadows and obscures the underlying structures (Figure 4B). Since PBM uses 50 nm particles to probe the surface of the object, those particles can easily probe underneath the overhang and inside the smiley face. PBM imaging clearly shows the smiley face structure as well as the overhang roof supported by a thick post (Figure 4C and D) with the sagittal cross section (Figure 4E). This allows PBM to capture not only the top surface of the object but also the internal cavity that is difficult for other nano-imaging techniques such as AFM and SEM.

These observations clearly prove that PBM enables wide-field optical imaging of complex, three-dimensional shapes with super-resolution in all three dimensions. The lateral resolution in PBM depends primarily on the localization precision of particles and their lateral diffusion lengths during single frame exposure time. The strong plasmon resonance of the metal NPs results in a couple of orders brighter PSFs (~25,000 photons) than when obtained with typical bright organic dye molecules employed in SMLM [18–21]. Thus, if they were stationary, localization precision [22, 23] of their lateral positions could be down to 5 nm at a typical per-frame exposure time of 1–5 ms. More dominant influence on lateral resolution is attributed to Brownian diffusion of particles that induces around 20–30 nm positional uncertainty in our typical exposure time. This error can be reduced with a shorter exposure time setting if allowed. For example, a 20× shorter pixel dwell time can be easily achieved with a 20× stronger laser source (~4 W) than used here, which still maintains much lower illumination power density onto samples than a few kW/cm^2 in typical fluorescence-based localization microscopy. A use of high-end back-illuminated scientific complementary metal-oxide-semiconductor cameras may further improve not only spatial resolution thanks to a higher signal-to-noise ratio and no excess noise like electron-multiplying charge-coupled device (EMCCD) cameras [23] but also temporal

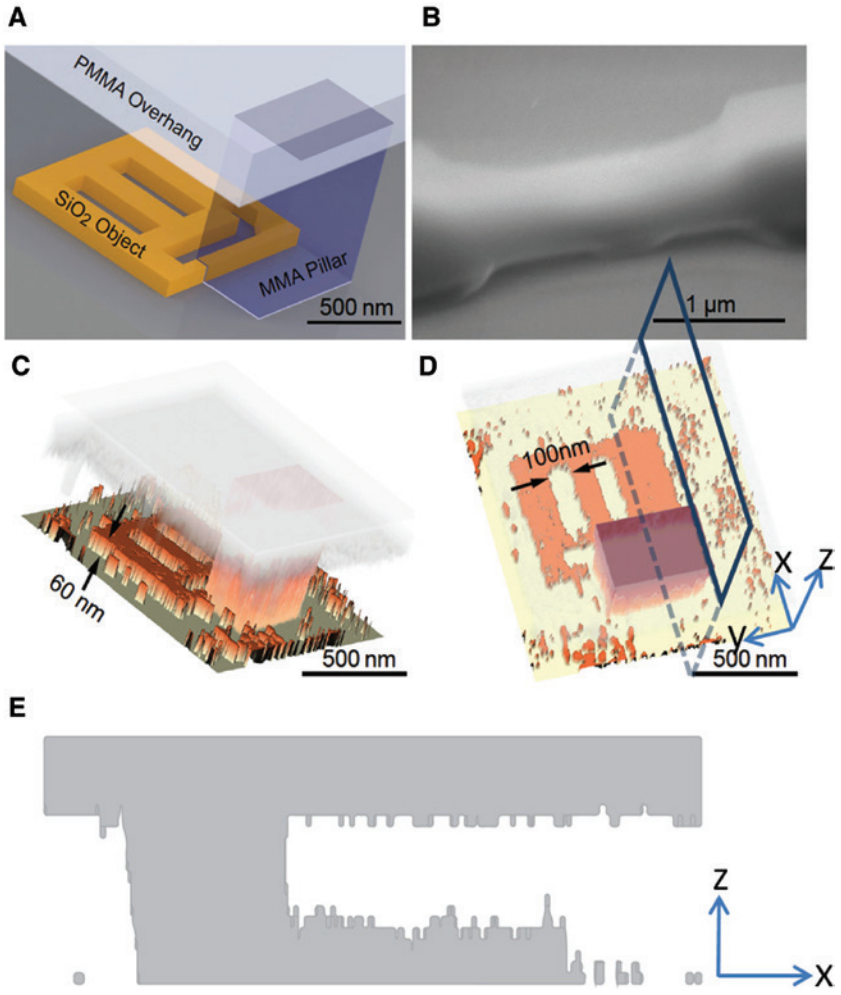

Figure 4: Imaging of topology of a three-dimensional shape with internal geometry.
(A) Schematic of the fabricated structure consisting of a silicon dioxide layer patterned onto a smiley face and an overhanging PMMA structure. The thick PMMA overhang (light gray), supported by the MMA post (blue) roofs the smiley SiO_2 face (yellow). (B) SEM image of the structure on which a small gap can be seen, but the top PMMA layer obscures the underlying smiley face. The MMA pillar can be distinguished in the middle. (C) Side view of the PBM reconstruction of the sample showing clearly the smiley (orange) face structure as well as the overhang roof (gray) supported by a thick post (orange). The image was reconstructed from 250,000 frames with 3 ms acquisition each and errors in determining height at certain positions are visible around the smiley face. (D) Top-down view of the sample showing that PBM was able to image 100 nm feature within the overhung structure. The rectangle represents a cutting plane which shows how the cross section in (E) was obtained. The dashed line and the solid line indicate the portion of the cutting plane that goes "through" and above the sample, respectively. (E) Sagittal (XZ) cross section of the reconstructed area where the cut plane is shown in (D). The gray areas correspond to the places where the sample is present (i.e. filled PMMA, while the white ones represent an empty space around the sample).

resolution due to their higher readout rate. The vertical resolution is mainly determined by the sensitivity of scattering intensity change through the particle's height set by TIR illumination, the axial diffusion distance, and uniformity of NPs. Each of these can be quite equally influential and therefore has to be minimized. For example, it is better to use a shallow evanescent field that extends only above the object. A higher uniformity of gold NPs needs to be used. We used a commercial 50 nm gold NPs (Ted Pella, originally from BBI, Redding, CA, USA) that are characterized as 55.6 ± 2.7 nm (see Supplementary Figure S1 in Supplementary Materials). Highly uniform gold NPs could be specially synthesized to minimize such axial uncertainty. We believe that other well-known strategies of axial localization such as highly axially dependent illumination, bi-plane detection or PSF engineering [24–26] will provide higher precision as these methods do not rely on the scattering intensity but the shape of PSFs over height. Thus, the illumination profile and the uniformity of NPs can become no longer critical. The axial diffusion is also minimized with a shorter exposure time under stronger illumination.

Our 3D imaging method would have an imaging depth of less than 1 μm mainly due to axial localization enabled by TIR illumination. However, thicker samples could also in principle be imaged in PBM by employing the aforementioned strategies [24–26]. Also, fluorescent particles rather than gold NPs could be considered in certain circumstances. Generally, however, such a fluorescence approach may show a limited capability of 3D imaging in PBM mainly due to relatively weaker signal intensity and possible bleaching effects. On the other hand, the surfaces of our demonstrated objects (made of PMMA and silica) and the functionalized gold NPs are all negatively charged (see the Methods section and Supplementary Materials for details). Hence, the NPs do not aggregate by themselves nor stick to the sample, which is prerequisite for PBM to work. Also, adding salt in the NP solution may promote an aggregation of the passivated NPs and thus has to be carefully decided if necessary for other purpose.

In conclusion, we proposed and demonstrated a proof of concept of PBM that harnesses a larger number of NPs as parallel scanning probes to achieve 3D super-resolution imaging over a larger area in a relatively short time compared with conventional SPM with a single probe. Under TIR illumination, 3D localization of NPs in Brownian motion around the object provides a 3D surface profile of nanoscale samples in label-free and bleaching-free ways. As demonstrated, PBM is capable of imaging a complex nanostructure with internal cavities. Typical samples compatible with PBM would be dielectric objects and the best imaging performance is achieved when the NP solution is index-matched to the object. PBM may be tolerant for a small index variation of <0.06 that exists within the object like biological cells or between the short object and the surrounding NP solution. Imaging metallic or plasmonic structures will be challenging in PBM because these samples can highly perturb TIR illumination as well as strongly interact with NPs. We believe that PBM's parallel scanning scheme much facilitates to visualize network nanostructures or biological objects compared with the demonstration of those by PFM with a single trapped particle [8, 9].

3 Methods

A prism-type home-built TIR setup was used in all experiments. A 5-mm-wide beam from a 200 mW 532-nm (~1 W/cm^2) laser is directed via mirrors arranged in periscope setting onto a triangular sapphire prism (n = 1.77) at an incident angle of around 60°. The laser's incident angle could be adjusted to make sure that the evanescent field covers a whole sample structure to be measured. The sample, mostly PMMA structures fabricated using electron beam lithography on cleaned thin sapphire or glass slide, is optically coupled to the top of the prism with immersion oil (n = 1.77, Cargille, Cedar Grove, NJ, USA). The evanescent wave with a penetration depth of ~100–250 nm is formed at the sapphire-PMMA interface and penetrates into the sample. A 2,2′-thiodiethanol-water (Sigma, St. Louis, MO, USA) [27] suspension, whose refractive index is matched to the sample (tuning range: 1.33–1.52), of 50 nm unconjugated gold NPs (15708-5, Ted Pella, Redding, CA, USA), passivated with bis(p-sulfonatophenyl)phenylphosphine dihydrate dipotassium salt (1 mg/ml, BSPP, Strem Chemicals, Newburyport, MA, USA) is placed on the top on the sample and sealed using a coverslip. The concentration of the particles is kept low enough so that the average distance between the particles is 0.5–1 μm. The imaging chamber is mounted on an inverted microscope (Zeiss Observer D1m, Carl Zeiss, Oberkochen, Germany), and laser light scattered from gold NPs is collected via 100× high NA objective (Nikon Apo TIRF, 1.49 NA, Nikon, Minato, Tokyo, Japan) and sent to an EMCCD camera (C9100, Hamamatsu, San Jose, CA, USA). Raw data are collected either via HCImage software (Hamamatsu, San Jose, CA, USA) or through a custom written LabView code (National Instruments, Austin, TX, USA). A typical exposure time of each frame is set to 1–5 ms. We record around 100,000 frames (total acquisition time: 300–500 s) that typically results in 20 particles per voxel. Each NP's image is fitted with a 2D Gaussian function with a constant background offset, from which the lateral position of the particle is found to be the center of the fitted function. The vertical position is also determined by the particle's fitted intensity (more rigorously integrated power) as the particle's scattering intensity is related to the exponentially decaying evanescent illumination. Further details on data analysis and 3D reconstruction are found in Supplementary Materials.

4 Supplementary material

The supplementary material is available online on the journal's website or from the author.

Acknowledgments: This work was supported by the Gordon and Betty Moore Foundation and the Office of Naval Research (ONR) MURI program under Grant No. N00014-13-1-0649. We thank Sui Yang for helping with the refractive index measurement of a PMMA film and Hoduk Cho

for helping with the transmission electron microscopy imaging of gold nanoparticles.

References

[1] Eaton P, West P. Atomic force microscopy. Oxford, UK, Oxford University Press, 2010.
[2] Taubner, T, Korobkin D, Urzhumov Y, Shvets G, Hillenbrand R. Near-field microscopy through a SiC superlens. Science 2006;313:1595.
[3] Villanueva G, Plaza JA, Sánchez-Amores A, et al. Deep reactive ion etching and focused ion beam combination for nanotip fabrication. Mater Sci Eng 2006;C26:164–8.
[4] Boisen A, Hansen O, Bouwstra S. AFM probes with directly fabricated tips. J Micromech Microeng 1996;6:58–62.
[5] Cheung CL, Hafner JH, Lieber CM. Carbon nanotube atomic force microscopy tips: direct growth by chemical vapor deposition and application to high-resolution imaging. Proc Natl Acad Sci USA 2000;97:3809–13.
[6] Minne S, Manalis S, Quate C. Parallel atomic force microscopy using cantilevers with integrated piezoresistive sensors and integrated piezoelectric actuators. Appl Phys Lett 1995;67:3918–20.
[7] Ahn Y, Ono T, Esashi M. Micromachined Si cantilever arrays for parallel AFM operation. J Mech Sci Technol 2008;22:308–11.
[8] Florin E-L, Pralle A, Hörber JKH, Stelzer EHK. Photonic force microscope based on optical tweezers and two-photon excitation for biological applications. J Struct Biol 1997;119:202–11.
[9] Tischer C, Altmann S, Fišinger S, Hörber JKH, Stelzer EHK, Florin E-L. Three-Dimensional thermal noise imaging. Appl Phys Lett 2001;79:3878–80.
[10] Dubois A, Grieve K, Moneron G, Lecaque R, Vabre L, Boccara C. Ultrahigh-resolution full-field optical coherence tomography. Appl Optics 2004;43:2874–83.
[11] Buma T, Norris TB. Time reversal three-dimensional imaging using single-cycle terahertz pulses. Appl Phys Lett 2004;84:2196–8.
[12] Jepsen PU, Cooke DG, Koch M. Terahertz spectroscopy and imaging – modern techniques and applications. Laser Photon Rev 2011;5:124–66.
[13] Fang N, Lee H, Sun C, Zhang X. Sub-diffraction-limited optical imaging with a silver superlens. Science 2005;308:534–7.
[14] Liu Z, Lee H, Xiong Y, Sun C, Zhang X. Far-field optical hyperlens magnifying sub-diffraction-limited objects. Science 2007;315:1686.
[15] Pendry J. Negative refraction makes a perfect lens. Phys Rev Lett 2000;85:3966–9.
[16] Ebbesen TW, Lezec HJ, Ghaemi HF, Thio T, Wolff PA. Extraordinary optical transmission through sub-wavelength hole arrays. Nature 1998;391:667–9.
[17] Dunn RC. Near-field scanning optical microscopy. Chem Rev 1999;99:2891–928.
[18] Huang B, Bates M, Zhuang X. Super-resolution fluorescence microscopy. Annu Rev Biochem 2009;78:993–1016.
[19] Lidke K, Rieger B, Jovin T, Heintzmann R. Superresolution by localization of quantum dots using blinking statistics. Opt Express 2005;13:1599–609.
[20] Rust M, Bates M, Zhuang X. Sub-diffraction-limit imaging by stochastic optical reconstruction microscopy (STORM). Nat Methods 2006;3:793–6.
[21] Betzig E, Patterson GH, Sougrat R, et al. Imaging intracellular fluorescent proteins at nanometer resolution. Science 2006;313:1642–5.
[22] Thompson RE, Larson DR, Webb WW. Precise nanometer localization analysis for individual fluorescent probes. Biophys J 2002;82:2775–83.
[23] Mortensen KI, Churchman LS, Spudich JA, Flyvbjerg H. Optimized localization analysis for single-molecule tracking and super-resolution microscopy. Nat Methods 2010;7:377–81.
[24] Dickson RM, Norris DJ, Tzeng YL, Moerner WE. Three-dimensional imaging of single molecules solvated in pores of poly(acrylamide) gels. Science 1996;274:966–8.
[25] Juette M, Gould T, Lessard M. Three-dimensional sub-100 nm resolution fluorescence microscopy of thick samples. Nat Methods 2008;5:527–9.
[26] Conkey DB, Trivedi RP, Pavani SR, Smalyukh II, Piestun R. Three-dimensional parallel particle manipulation and tracking by integrating holographic optical tweezers and engineered point spread functions. Opt Express 2011;19:3835–42.
[27] Staudt T, Lang MC, Medda R, Engelhardt J, Hell SW. 2,2′-Thiodiethanol: a new water soluble mounting medium for high resolution optical microscopy. Micros Res Tech 2007;70:1–9.

Supplemental Material: The online version of this article offers supplementary material (https://doi.org/10.1515/nanoph-2017-0075).